Adapting to oxygen: 3-Hydroxyanthrinilate 3,4-dioxygenase employs loop dynamics to accommodate two substrates with disparate polarities

Received for publication, March 1, 2018, and in revised form, May 18, 2018 Published, Papers in Press, May 21, 2018, DOI 10.1074/jbc.RA118.002698

Yu Yang[‡], **Fange Liu**[§1], **and Aimin Liu**[‡2]

From the [‡]*Department of Chemistry, University of Texas at San Antonio, San Antonio, Texas 78249 and the* [§]*Department of Biochemistry and Biophysics, Perelman School of Medicine, University of Pennsylvania, Philadelphia, Pennsylvania 19104*

Edited by F. Peter Guengerich

3-Hydroxyanthranilate 3,4-dioxygenase (HAO) is an iron-dependent protein that activates O_2 and inserts both oxygen atoms into 3-hydroxyanthranilate (3-HAA). An intriguing question is how HAO can rapidly bind O_2, even though local O_2 concentrations and diffusion rates are relatively low. Here, a close inspection of the HAO structures revealed that substrate- and inhibitor-bound structures exhibit a closed conformation with three hydrophobic loop regions moving toward the catalytic iron center, whereas the ligand-free structure is open. We hypothesized that these loop movements enhance O_2 binding to the binary complex of HAO and 3-HAA. We found that the carboxyl end of 3-HAA triggers changes in two loop regions and that the third loop movement appears to be driven by an H-bond interaction between Asn[27] and Ile[142]. Mutational analyses revealed that N27A, I142A, and I142P variants cannot form a closed conformation, and steady-state kinetic assays indicated that these variants have a substantially higher K_m for O_2 than WT HAO. This observation suggested enhanced hydrophobicity at the iron center resulting from the concerted loop movements after the binding of the primary substrate, which is hydrophilic. Given that O_2 is nonpolar, the increased hydrophobicity at the iron center of the binary complex appears to be essential for rapid O_2 binding and activation, explaining the reason for the 3-HAA–induced loop movements. Because substrate binding-induced open-to-closed conformational changes are common, the results reported here may help further our understanding of how oxygen is enriched in nonheme iron-dependent dioxygenases.

It is estimated that ~30% of the mass of woody plant material on earth is comprised of aromatic compounds that are known for their unusual stability when compared with similar aliphatic hydrocarbons (1). One strategy devised by nature to overcome the stability of aromatic compounds is to utilize iron-bound oxygen directly to cleave the ring, breaking aromaticity. The ring-cleaving dioxygenase enzymes are abundant and versatile. These enzymes utilize a mononuclear, nonheme iron ion to orchestrate electron transfer between an organic substrate and oxygen molecule with catalytic reaction rates rapid enough for their catalytic intermediates to escape spectroscopic characterization (2). A fundamental question is how these enzymes accomplish rapid O_2 binding, a prerequisite for the observed catalytic rates, whereas local O_2 concentrations in aqueous solution are relatively low (200–300 μM at 1 atm pressure and room temperature), and the rate of oxygen diffusion from air to solution is slow relative to the rate of catalysis.

Here, we chose 3-hydroxyanthranilate 3,4-dioxygenase (HAO),[3] a ring-cleaving dioxygenase, as a model system to study this problem. HAO is a nonheme, iron-dependent extradiol dioxygenase belonging to the cupin superfamily (3–5). This enzyme cleaves the aromatic ring of its substrate adjacent to the substitution groups. It activates and inserts dioxygen between C3 and C4 of its substrate 3-hydroxyanthranilate (3-HAA), ultimately producing quinolinic acid via the intermediary product α-amino-β-carboxymuconate-ϵ-semialdehyde (Fig. 1*A*). HAO is present in the kynurenine pathway, where it is essential for tryptophan degradation and *de novo* NAD^+ biosynthesis in eukaryotic organisms and a few bacteria (6–10). This enzyme is also found in the 2-nitrobenzoic acid catabolic pathway for energy production in some bacteria (11). HAO from *Cupriavidus metallidurans* has been shown to operate at a catalytic turnover rate of 25 s^{-1} (3, 12) until near depletion of O_2. A second iron-binding site at the protein surface has been proposed to be an iron storage site for the protein to ensure active-site iron occupancy when the enzyme is dealing with a substrate that is also a metal chelator (13).

Previous structural studies of HAO have allowed atomic level understanding of the overall protein structure and the active

This work was supported in part by National Science Foundation Grant CHE-1623856 (to A. L.) and National Institutes of Health Grants GM107529, GM108988, and MH107985 (A. L.). The authors declare that they have no conflicts of interest with the contents of this article. The content is solely the responsibility of the authors and does not necessarily represent the official views of the National Institutes of Health.

The atomic coordinates and structure factors (codes 6BVP, 6BVQ, 6BVR, 6BVS, 6CD3, 6D60, 6D61, and 6D62) have been deposited in the Protein Data Bank (http://wwpdb.org/).

This article contains Figs. S1–S10.

[1] To whom correspondence may be addressed. Tel.: 215-573-6413; E-mail: liufg@pennmedicine.upenn.edu.

[2] To whom correspondence may be addressed. Tel.: 210-458-7062; E-mail: Feradical@utsa.edu.

[3] The abbreviations used are: HAO, 3-hydroxyanthranilate dioxygenase; 3-HAA, 3-hydroxyanthranilate; ClHAA, 4-Cl-3-HAA; PDB, Protein Data Bank; wtHAO, WT HAO; RMSD, root-mean-square deviation; αKG, α-ketoglutarate; PAH, phenylalanine hydroxylase.

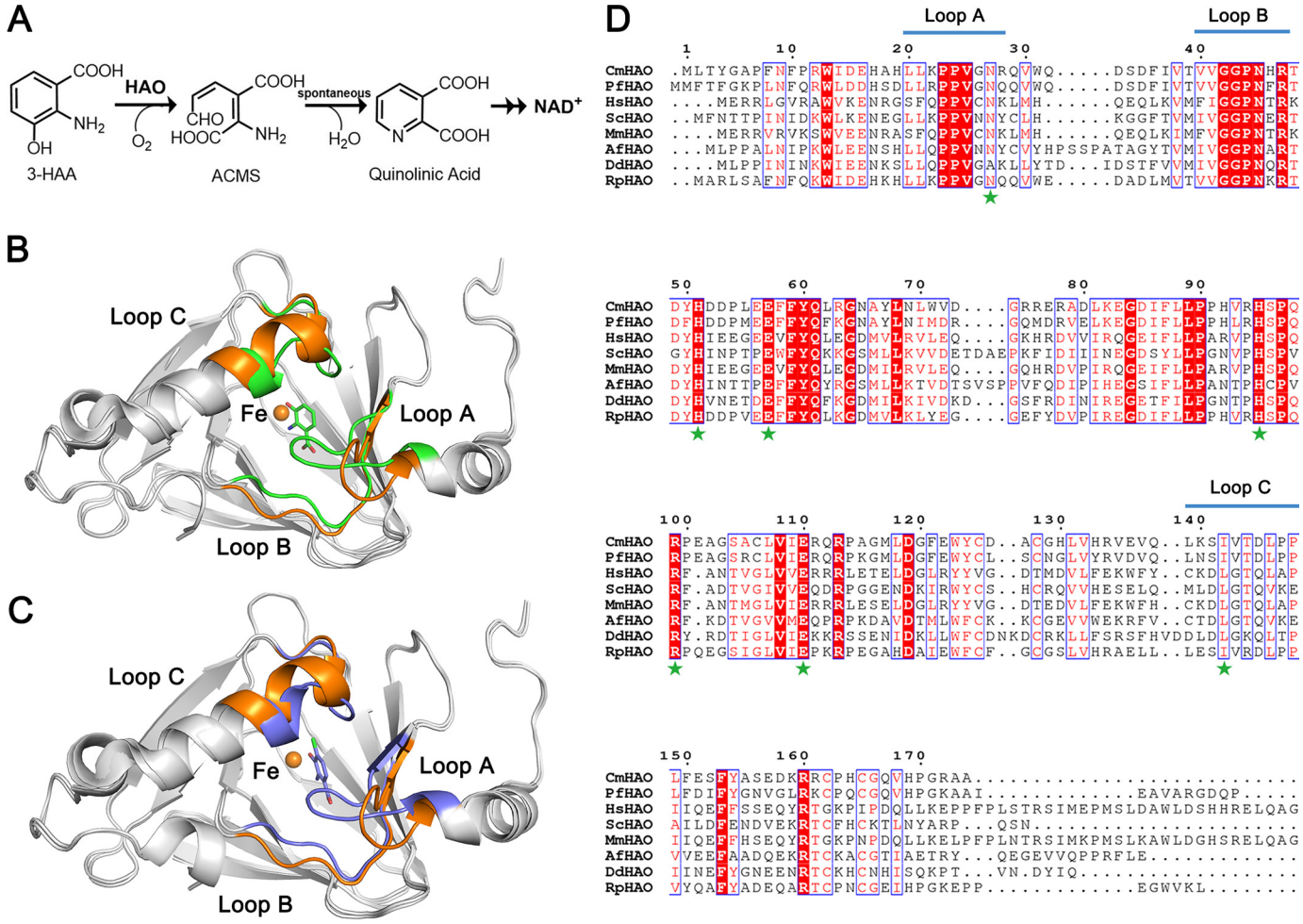

Figure 1. Loop region identification and HAO sequence alignment. *A*, scheme of NAD^+ synthesis from kynurenine pathway. *B* and *C*, comparison of overall structures and colored loop regions in the ligand-free (*orange*, PDB entry 4L2N), 3-HAA-bound (*green*, PDB entry 1YFY), and ClHAA-bound (*purple*, PDB entry 1YFW) wtHAO; the catalytic iron molecules (*Fe*) are shown as the *orange balls*. *D*, alignment of HAO active-site center region sequences from *C. metallidurans* (ABF12052), *Pseudomonas fluorescens* (BAC65311), *H. sapiens* (P46952), *S. cerevisiae* (P47096), *Mus musculus* (Q78JT3), *Aspergillus fumigatus* Af293 (XP_747271), *Dictyostelium discoideum* AX4 (XP_640237), and *Ruegeria pomeroyi* DSS-3 (AAV95053). The conserved residues are *boxed* in *blue* (31), and their similar residues are highlighted by *red shading*. The essential residues around the active site are marked by *green stars*. The loop regions are labeled on the *top* with *blue bars*.

site architecture (3–5). A substrate analog, 4-Cl-3-HAA (ClHAA) was tested and defined as an irreversible inhibitor to prevent the active site from binding with the native substrate (12). The crystal structures of HAO from *C. metallidurans* were also reported previously (3, 13). In this study, a closer inspection of the substrate-free (PDB entry 4L2N) and substrate-bound (PDB entry 1YFY) structures of WT HAO (wtHAO) showed that the enzyme exhibits two distinct conformations (Fig. 1*B*), which are hereafter termed open and closed states. The substrate-bound structure is in the closed conformation, showing significant structural differences relative to the ligand-free, open state of three specific loop regions surrounding the catalytic iron center, which is composed of a ferrous ion coordinated by a His_2–Glu_1 motif. The crystal structure of HAO in complex with O_2 and ClHAA (PDB entry 1YFW) (3, 12) also shows the closed state with three loops moving toward the active site (Fig. 1*C*). Therefore, the questions raised here are the following: 1) What is the driving force for the loop movement? 2) How are the loop movements on the three loop regions coordinated? 3) What is the potential biological significance of the loop movement in the context of oxygen binding? To investigate these questions, we identified and mutated the essential residues involved in the loop movement, determined kinetic parameters for both oxygen and 3-HAA, and performed X-ray crystallographic studies. The results revealed how the nonheme iron enzyme handles its substrates with disparate polarities through a primary substrate-induced change of the active site hydrophobicity.

Results

Insights inferred from sequence and structural alignments

We noted that three largely hydrophobic loop regions in HAO move toward the catalytic iron center, forming a closed conformation upon HAO binding with the primary substrate (PDB entry 1YFY) compared with the ligand-free counterpart (PDB entry 4L2N) (3, 13). Similar structural features were obtained in hundreds of repeated data sets of the ligand-free and substrate-bound structures, indicating that the organic substrate-binding induced closed conformation is an intrinsic feature of the enzyme. The three loop regions consist of residues 21–28 for loop region A (**Leu^{20}-Leu^{21}**-Lys^{22}-**Pro^{23}**-

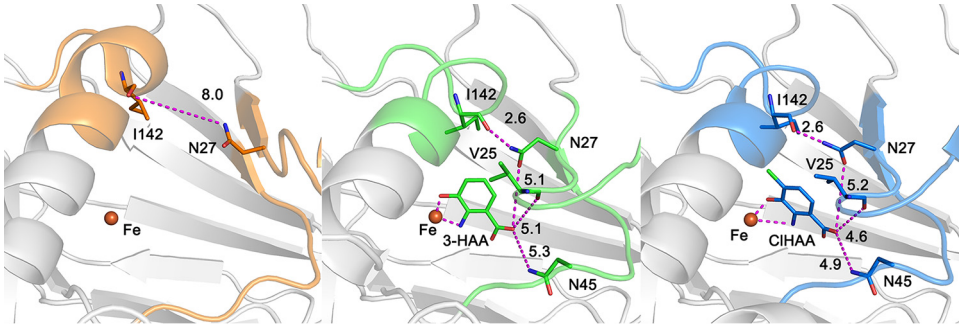

Figure 2. The positions and interactions between Ile^{142} and Asn^{27} of ligand-free HAO (*left*), 3-HAA-bound HAO (*middle*), and ClHAA-bound HAO (*right*). The three loop regions involved in loop-movement are highlighted in *color*. Ile^{142}, Asn^{27}, Val^{27}, Asn^{45}, and 3-HAA are shown as *sticks*. The distances between two-atom pairs are measured in units of Å and shown in *dashed lines*.

Pro^{24}-Val^{25}-Gly^{26}-Asn^{27}-Arg^{28}), 40–47 for loop region B (**Val^{40}-Val^{41}-Gly^{42}-Gly^{43}-Pro^{45}**-His^{46}-Arg^{47}), and 139–148 for loop region C (**Leu^{139}**-Lys^{140}-Ser^{141}-**Ile^{142}-Val^{143}**-Thr^{144}-Asp^{145}-**Leu^{146}-Pro^{147}-Pro^{148}**). Most of these residues are highly conserved across the protein sequences of HAO from various origins (Fig. 1*D*).

A salient feature is that all three loops are composed of mostly hydrophobic residues (bolded); 17 of the total 26 residues (65%) are aliphatic (Fig. S1). Each loop also contains one or two proline residues. Proline is a cyclic hydrophobic residue and is commonly utilized as a helix breaker and an aid in formation of turns. Two consecutive proline residues are present in both loop A and loop C (*i.e.* Pro^{23}-Pro^{24} and Pro^{147}-Pro^{148}, respectively). The proline fragment endows the two loops with increased hydrophobic structure. It is interesting to note that the two negatives make a positive, *i.e.* the Pro^{147}-Pro^{148} fragment, a double helix breaker, is part of an α-helical structure. Loop B is a highly hydrophobic fragment with only one proline residue (Pro^{45}). Upon 3-HAA binding-induced loop movement, loop A undergoes the largest movement among the three loops with a shift toward the active site of ~8.6 Å in average when compared with the corresponding loop regions in the substrate-free form.

Another notable feature of the loop regions in the closed form of HAO is that the side chains of hydrophobic residues of Val^{25}, Val^{41}, Ile^{142}, Val^{142}, Leu^{139}, and Leu^{146} are sequestered toward to the active site, where the catalytic iron ion is located (Fig. S1, *B* and *D*). Meanwhile, most of the side chains of the hydrophilic residues point away from the active site: Lys^{22}, Arg^{28}, His^{46}, Lys^{140}, Thr^{144}, and Asp^{145} (Fig. S1, *B* and *C*). When the three loops are gathered toward the catalytic iron ion, the ligand-bound iron center becomes significantly more compact and hydrophobic, which is distinct with respect to the more open and spacious conformation observed in the ligand-free structure. The movement of loop A is triggered by the interaction of the substrate carboxylate group with the side chains of Asn^{27} and Asn^{45} and the backbone of Val^{25}, which form the potential H-bond or salt-bridge network in both substrate-bound and ClHAA-bound structures (Fig. 2). Loops A and B appear to move synergistically because of the nearly pairwise backbone residue interactions and like a "double-door" to the active site cavity. As shown in Fig. S1*C*, an H-bonding network forms among the backbones of residues Pro^{23}, Pro^{24}, and Gly^{26} in loop A and Gly^{42}, Pro^{44}, and His^{46} in loop B, gathering loops A and B toward the active site.

Single-point mutation of Asn^{27} and Ile^{142} diminished the catalytic efficiency by decreasing the oxygen capturing capacity

One question arising from the structural comparison is how loop C is triggered to move toward the catalytic iron center. This loop region is more distant from the active site in the open conformation. However, the entire α-helix to which loop C is connected rotates ~10° (Fig. S1*B*). After binding 3-HAA or ClHAA, the side chain of Asn^{27} and the backbone of Ile^{142} moves closer to the iron center by forming hydrogen-bonding interactions with each other (Fig. 2) (3). Specifically, the distance between the backbone amide of Ile^{142} from loop C and the side chain of Asn^{27} from loop A decreases substantially, from ~8.0 to 2.6 Å, which results in loops A and C directly moving together and toward the active site. Thus, Asn^{27} and Ile^{142} appear to be the critical residues for a coordinated conformational change during 3-HAA binding to the iron ion.

To determine the connection and especially the effect of the loop movement on the reaction catalyzed by HAO, we mutated Asn^{27} and Ile^{142} to proline and alanine. The kinetic parameters of N27A, I142P, and I142A were determined for both substrates, 3-HAA and O_2 in separate experiments. With respect to the organic substrate, 3-HAA, two different buffer environments were involved. One was the oxygen-saturated buffer by bubbling oxygen (>1.3 mM) during measurement, and the other used regular buffer without any treatment and contained 286 ± 8 μM molecular oxygen. Under the regular buffer environment, the mutant N27A showed a 6-fold decrease in the k_{cat} and a 7-fold increase in the K_m (3-HAA) relative to the WT enzyme (Table 1), exhibiting a substantially reduced catalytic efficiency, 2.5% of wtHAO. However, using O_2 saturated buffer, the k_{cat} of N27A reached the same level of wtHAO, indicating that the primary reason for a substantial negative impact of the N27A mutation in catalysis with the regular buffer is a decreased oxygen-binding affinity.

The I142A and I142P variants showed 53- and 9.5-fold decreased catalytic efficiency, k_{cat}/K_m, toward 3-HAA with the regular buffer compared with wtHAO, respectively. The $K_{m\ (3\text{-HAA})}$ (239.7 μM) of I142A increased 10-fold, whereas the k_{cat} decreased by ~5-fold compared with these of wtHAO.

Table 1
Kinetic constants of the wild-type and mutants of HAO with 3-HAA

Enzyme	Buffer	Substrate	K_m	k_{cat}	$k_{cat}/K_m \times 10^3$
			μM	s^{-1}	$s^{-1}\ \mu M^{-1}$
Wild-type[a]		3-HAA	22.4 ± 2.7	25	1120 ± 130
Wild-type	O_2 saturated[b]	3-HAA	24.7 ± 4.7	24.2 ± 2.3	980 ± 210
N27A	O_2 (286 μM)	3-HAA	142 ± 18	3.97 ± 0.3	28.0 ± 4.1
N27A	O_2 saturated[b]	3-HAA	72.0 ± 9.2	26.5 ± 1.8	368 ± 53
I142A	O_2 (286 μM)	3-HAA	240 ± 50	5.01 ± 0.6	20.9 ± 5.0
I142A	O_2 saturated[b]	3-HAA	110 ± 20	13.9 ± 0.9	126 ± 25
I142P	O_2 (286 μM)	3-HAA	97 ± 15	11.5 ± 0.7	118 ± 20
I142P	O_2 saturated[b]	3-HAA	187 ± 34	24.8 ± 2.6	133 ± 28
Wild-type	3-HAA saturated[c]	O_2	156 ± 36	25.8 ± 2.8	165 ± 42
N27A	3-HAA saturated[c]	O_2	1144 ± 48	15.7 ± 0.5	13.64 ± 0.7
I142A	3-HAA saturated[c]	O_2	>2227	>19.5	ND
I142P	3-HAA saturated[c]	O_2	1120 ± 250	21.3 ± 3.4	19.0 ± 5.2

[a] Values from a previous study (3).
[b] The saturated O_2 concentration is more than 1.3 mM.
[c] The concentration of 3-HAA for wtHAO is 200 μM and for two mutants is 600 μM.

The $K_{m\ (3\text{-HAA})}$ of I142P increased 4.3-fold. With oxygen-saturated buffer, the apparent constants k_{cat} of I142A and I142P for 3-HAA are 13.9 ± 0.9 and 24.8 ± 2.6 s^{-1}, respectively, showing a partial or a full rescue of the catalytic efficiency. Interestingly, both mutants exhibited a near comparable catalytic activity with that of wtHAO only with oxygen supplementation.

Because of the apparent yet significant increasing of hydrophobic environment in the active site, we hypothesize that the major benefit of the loop movement is to attract the other nonpolar substrate, molecular oxygen. We also determined the K_m value of O_2. With a saturating amount of 3-HAA, the K_m value increased ~9-fold, from 124.8 μM for wtHAO to 1144 μM for N27A and 1120 μM for I142P, whereas the k_{cat} remained similar (Table 1). An attempt to determine the K_m for O_2 of I142A mutant failed because of an inability to saturate the enzyme (K_m > 2,227 μM).

Mutation of Asn^{27} evades substrate-binding–induced loop movement

To assess whether or not the closed conformation would still be formed upon substrate binding after the alteration of the primary residue involved in orchestrating the loop movement, the mutant N27A was crystallized under similar conditions reported for wtHAO (3, 13). The holo crystal structures of N27A in the ligand-free form was refined to 1.90 Å (Table 2). Comparison of the structure of N27A (Fig. 3*A*) with wtHAO (PDB entry 4L2N) revealed no apparent deviations, including the metal ligands and second sphere residues, as indicated by a small RMSD value of 0.090 Å between the two structures of all Cα carbons. We then attempted to obtain a ligand-bound structure of this mutant. N27A crystals were soaked with 3-HAA or ClHAA anaerobically. The crystal structure of N27A in complex with ClHAA was solved at 2.30 Å (Fig. 3*B*). The omit map in the active site clearly illustrates the location of carboxylate and amine groups of ClHAA because of its strong salt-bridge interactions with residue Arg^{99} (Fig. S2). However, the phenyl ring and chloride electron densities were incomplete. Compared with ClHAA-bound wtHAO structures (PDB entries 1YFW and 1YFX), there is also negative density map around the chloride of ClHAA (3). Unfortunately, the ES complex structure remained elusive, even after extensive attempts. Compared with the single-crystal electronic absorption spectrum of ligand-free N27A, a N27A crystal soaked with ClHAA for 5 min exhibits an apparent absorbance peak at 328 nm (Fig. 3*C*), which is characteristic of ClHAA, indicating that ClHAA is indeed bound to N27A. The solution state UV-visible spectra of ClHAA-bound wtHAO and N27A showed similar binding affinity for the inhibitor (Fig. S3). The absorbance maximum of the inhibitor is also centered around 328 nm, which agrees well with the single-crystal UV-visible data.

The electron density map of ClHAA-bound N27A reveals that the inhibitor binds to the active-site iron with an iron-hydroxyl distance of 2.7 Å, similar to what was observed in the ClHAA-bound structure of wtHAO. However, the superimposition of ClHAA-bound N27A and wtHAO structures reveals several differences. As compared with wtHAO, the phenyl ring of the inhibitor moved up with an angle of 23° in the mutant structure, whereas the carboxylate group was fixed in both structures by a salt bridge with Arg^{99}, and the hydroxyl group of the inhibitor was stabilized by an H-bond with side chain of Glu^{110}. Both the open form model (PDB entry 4L2N) and the closed form model (PDB entry 1YFW) were utilized to build the loop regions. The results showed that the density map of loop regions could only fit with the model of open form. Unlike wtHAO, binding of ClHAA to N27A did not lead to the closed state and did not induce the loop movement. The loop regions could be well aligned with the substrate-free wtHAO (Fig. 3, *D* and *E*). The distance between the backbone of Ile^{142} and Ala^{27} in the complex structure (9.9 Å) was not significantly different from that of the ligand-free wtHAO structure and not eligible to form a direct interaction. These results reveal the molecular details that support the hypothesis by which the interaction between Asn^{27} and Ile^{142} is the key link to bring the loop regions together toward the catalytic iron center. The incompleted density map of ClHAA in Fig. 3*B* might be due to the multiple conformations of phenyl ring and chloride of ClHAA in the open form of the active site.

Effect of Ile^{142} on loop regions conformation change

Because the mutation of Ile^{142} to proline and alanine also significantly decreased the oxygen binding and activation capacity (Table 1), a question raised was whether I142P and I142A would also be incompetent to present a closed conformation after binding with the substrate or ClHAA. Considering the H-bond interaction is observed between the backbone of Ile^{142} and the side chain of Asn^{27}, the I142A mutant was

Table 2
Crystallization data collection and refinement statistics

	HAO N27A ligand-free	HAO N27A ClHAA-bound	HAO I142A ligand-free	HAO I142A ClHAA-bound	HAO I142A 3-HAA-bound	HAO I142P ligand-free	HAO I142P ClHAA-bound	HAO I142P 3-HAA-bound
Data collection								
Space group	$P6_522$	$P6_522$	$P6_522$	$P6_522$	$P6_522$	$P6_522$	$P6_522$	$P6_522$
Cell dimensions *a*, *b*, *c* (Å)	58.4, 58.4, 230.5	58.6, 58.6, 236.3	58.9, 58.9, 232.1	58.3, 58.3, 239.6	58.4, 58.4, 230.8	58.5, 58.5, 232.2	58.7, 58.7, 231.9	58.9, 58.9, 232.3
Resolution	50–1.90 (1.97–1.90)[a]	50–2.10 (2.18–2.10)	50–1.90 (1.93–1.90)	50–2.31 (2.35–2.31)	50–2.60 (2.64–2.60)	50–2.22 (2.26–2.22)	50–1.74 (1.77–1.74)	50–1.77 (1.80–1.77)
No. of observed reflections	19,292 (1816)	14,268 (1466)	20,024 (946)	10,918 (519)	7693 (350)	12,593 (620)	25,473 (1160)	24,171 (1151)
Redundancy	10.3 (5.7)	28.7 (31.4)	10.8 (8.2)	17.6 (19.0)	15.2 (7.5)	22.5 (22.6)	26.1 (21.2)	9.9 (9.0)
Completeness (%)	99.4 (97.3)	100 (94.3)	99.9 (99.3)	99.9 (99.8)	98.4 (87.1)	99.8 (100)	99.5 (92.9)	98.6 (97.9)
$I/\sigma(I)$	16.7 (1.6)	8.8 (10.3)	22.9 (3.6)	17.9 (3.7)	19.0 (2.2)	21.9 (4.8)	42 (3.2)	30.2 (5.5)
R_{merge} (%)[b]	17.1 (52.2)	23.6 (39.4)	11.8 (38.2)	21.1 (93.3)	17.8 (43.9)	18.4 (95.4)	10.1 (90.9)	8.2 (31.4)
$CC_{1/2}$[c]	0.99 (0.85)	0.98 (0.98)	1.00 (0.98)	0.99 (0.97)	1.00 (0.93)	1.00 (0.98)	1.00 (0.97)	1.00 (0.99)
Refinement[d]								
R_{work}	19.2	22.8	19.2	20.5	19.2	20.8	19.9	18.7
R_{free}	23.2	26.7	24.1	25.5	24.9	25.2	23.7	21.6
RMSD bond length (Å)[e]	0.007	0.011	0.007	0.009	0.007	0.008	0.006	0.006
RMSD bond angles (°)	0.830	0.935	0.896	0.901	0.974	1.174	0.802	0.848
Ramachandran statistics[f]								
Preferred (%)	98.2	97.6	98.3	98.8	97.6	98.3	99.4	98.8
Allowed (%)	1.2	2.4	1.7	1.2	1.2	1.7	0.6	1.2
Outliers (%)	0	0	0	0	1.2	0	0	0
Average B-factor (Å^2)								
Protein/atoms	38.7/1382	44.4/1377	40.0/1428	45.8/1401	31.3/1377	35.3/1408	27.5/1408	21.9/1414
ClHAA or 3-HAA/atoms	NA[g]	53.7/12	NA	62.8/12	38.0/11	NA	30.1/12	22.9/11
Tris/atoms	49.3/8	47.6/8	39.2/8	53.8/8	NA	39.0/8	31.0/8	30.6/8
Iron/atoms	42.4/2	58.4/2	36.6/2	59.6/2	26.2/2	48.8/2	33.4/2	28.8/2
Solvent/atoms	47.2/143	47.8/96	46.5/181	45.9/68	28.9/63	37.8/144	37.8/264	33.0/298
PDB code	6BVP	6BVQ	6BVR	6BVS	6CD3	6D60	6D61	6D62

[a] Values in parentheses are for the highest resolution shell.
[b] $R_{merge} = \Sigma_{hkl}\Sigma_i|I_i(hkl) - I(hkl)|/\Sigma_{hkl}\Sigma_i I_i\,(hkl)$, in which the sum is over all the *i* measured reflections with equivalent Miller indices *hkl*, *I*(*hkl*) is the averaged intensity of these *i* reflections, and the grand sum is over all measured reflections in the data set.
[c] According to Karplus and Diederichs (28).
[d] All positive reflections were used in the refinement.
[e] According to Engh and Huber (29).
[f] Calculated by using MolProbity (30).
[g] NA, not applicable.

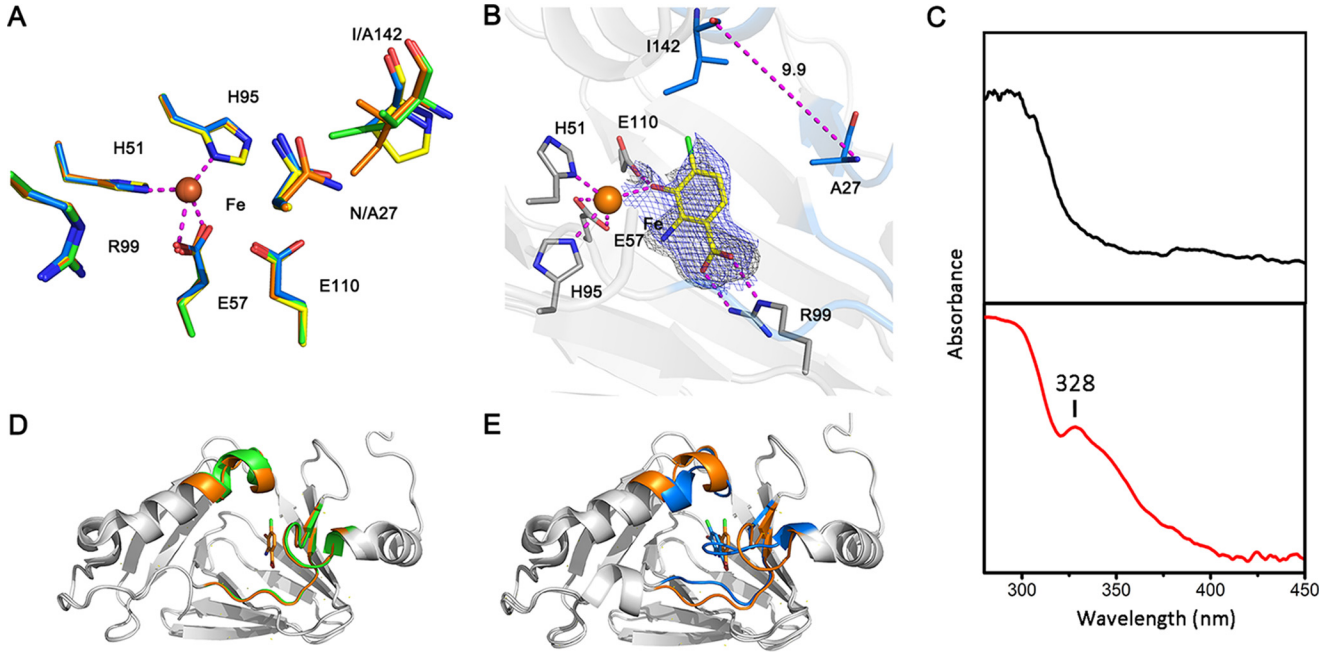

Figure 3. The mutant N27A disabled ClHAA-induced loop movement. *A*, comparison of active site residues in ligand-free structure of wtHAO (*orange*) and N27A (*green*) and I142A (*blue*) mutants. *B*, ClHAA-bound structure of N27A. The residues of active site are *gray*, Ala[27] and Ile[142] are *blue*, the inhibitor is *yellow*, and the $2F_o - F_c$ (*gray*) and $F_o - F_c$ (*blue*) maps for ClHAA are contoured at 1 and 2.5 σ, respectively. *C*, single-crystal electronic absorption spectra of the ligand-free (*top panel*) and ClHAA-bound (*bottom panel*) of N27A mutant. *D*, comparison of loop regions in wtHAO (*green*) and ClHAA-bound N27A mutant (*orange*). *E*, comparison of loop regions in ClHAA-bound wtHAO (*blue*) and ClHAA-bound N27A mutant (*orange*).

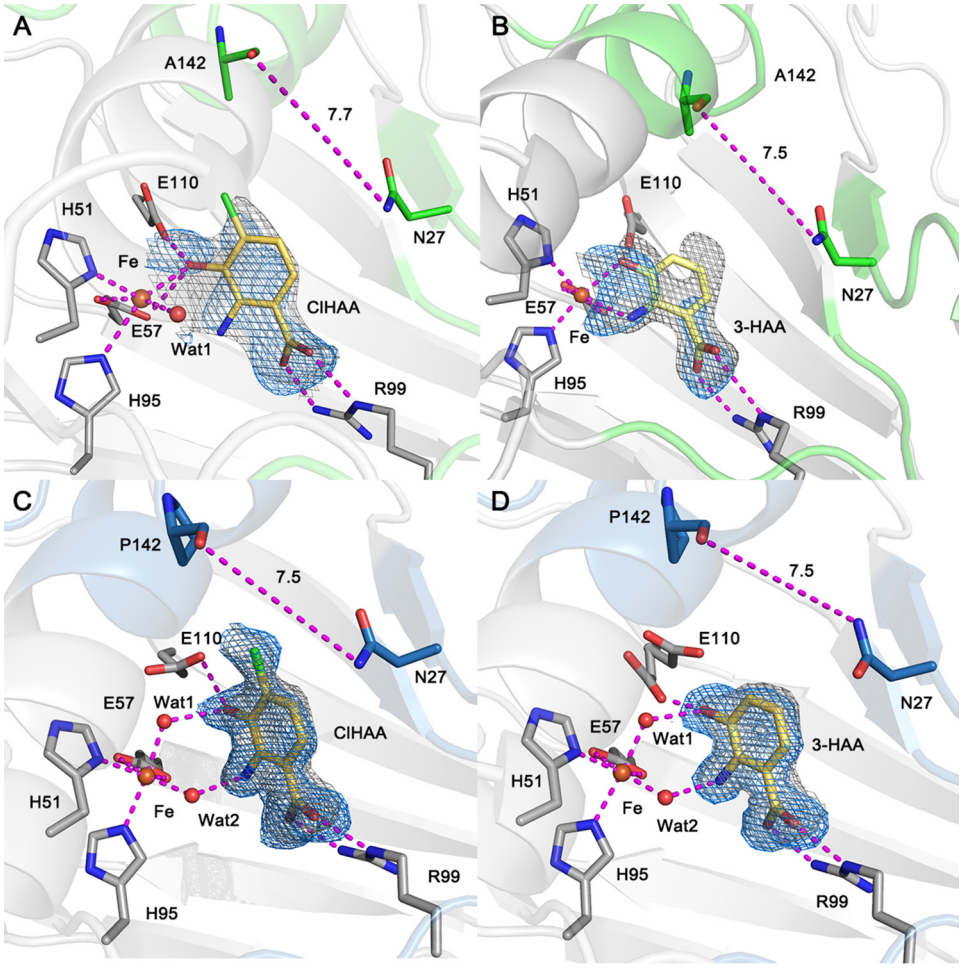

Figure 4. The complex structures of Ile^{142} mutants with ClHAA or 3-HAA. *A* and *B*, the ClHAA– and 3-HAA–bound I142A structures. *C* and *D*, the ClHAA– and 3-HAA–bound I142P structures. Active site residues are shown in *gray*, and ClHAA and 3-HAA are shown in *yellow*. The Asn^{27} and Ala^{142} are shown in *blue* in *A* and *B*, and Asn^{27} and Pro^{142} are shown in *green* in *C* and *D*. The $2F_o - F_c$ (*gray*) and $F_o - F_c$ (*blue*) maps for ClHAA and 3-HAA are contoured at 1 and 2.5 σ, respectively.

expected to have a more subtle effect than N27A or I142P mutants on the oxygen binding and activation efficiency. The potential effects of deletion of the side chain of Ile^{142} on loop regions movement were investigated by solving the ligand-free, enzyme–substrate, and enzyme–inhibitor complex structures.

The superimposed ligand-free structures of I142A (resolution 1.90 Å) and I142P (resolution 2.22 Å) and wtHAO showed high similarity with an RMSD of 0.141 and 0.161 Å from all the Cα atoms aligned in these structures. After soaking with ClHAA for 10 min, an I142A–ClHAA complex was obtained and refined at 2.31 Å (Fig. 4*A* and Fig. S4). The single-crystal electronic absorption spectrum of the I142A crystal soaked with ClHAA shows absorbance at 328 nm caused by binding of the inhibitor to the HAO variant (Fig. S5). Like the N27A mutant, the overall structure of the I142A–ClHAA complex also exhibited high similarity with wtHAO with an RMSD of 0.144 Å. The binding mode of ClHAA to the active-site iron ion of I142A was identical to the N27A–ClHAA complex except that a water molecule is still bound to iron ion. However, the distance between the side chain of Asn^{27} and Ala^{142} backbone was 7.7 Å, making it too far to form a hydrogen-bond interaction. Three loop regions of the I142A–ClHAA complex align well with the open form of ligand-free wtHAO structure (PDB entry 4L2N in Fig. S6). Moreover, the crystal structure of I142A in complex with 3-HAA was obtained and refined to 2.60 Å (Fig. 4*B*). The electron density map reveals that 3-HAA binds to the active site of I142A in a bidentate chelation pattern. The superimposition of these two structures reveals a 45° rotation of the phenol rings of the substrates in the active site. The loop regions can be well aligned with the substrate-free structure (Fig. S6). The distance between Ala^{142} and Asn^{27} is 7.6 Å, not eligible for formation of an H-bond.

We also crystallized I142P and soaked its crystals with 3-HAA and ClHAA. As a result, the complex structures of I142P bound with 3-HAA or ClHAA were determined and refined to high resolution (Table 2). Fig. 4 (*C* and *D*) clearly show a completed omit density map for both of ClHAA and 3-HAA in a similar binding mode to each other in the active site but distinct from those observed for the wtHAO. The ligands are anchored in the active site by interacting with the side chains of Arg^{99} and Glu^{110}. However, they are not directly ligated to the catalytic iron ion. Additionally, the two water ligands remain coordinated to the metal ion. Because residue 142 is part of an α-helix structure, and it sits at the start point of the loop C region, the helical structure of I142P in loop C is shorter than that of the wtHAO, resulting in a relatively larger

change of the loop C than that in I142A. However, the overall structures of ClHAA- and 3-HAA-bound I142P show high similarity to wtHAO with an RMSD of 0.180 and 0.166 Å, respectively. Moreover, the loop regions well align with the substrate-free, open-form of wtHAO despite a shorter helix in loop C (Fig. S7). The distances for the two complexes between Pro^{142} and Asn^{27} are 8.5 and 8.4, respectively, and hence these residues are not able to interact with each other. Of note, the I142P alteration leads to a new binding mode for 3-HAA and ClHAA, which explains the 330-to-350 nm shift of the absorbance maximum in the ClHAA-bound I142P solution optical spectrum (Fig. S3).

A perusal of the differences between the open and closed forms of HAO revealed that not only does the backbone of Ile^{142} form a hydrogen bond with Asn27 in the closed form, but its bulky, hydrophobic side chain also points toward the active site. Compared with the ligand-free structure, deletion of the side chain of Ile^{142} led to a larger cavity with seven ordered water molecules between Ala^{142} and the iron center in the ligand-free structure (Fig. S8). The I142P structure also has extra solvent between the Pro^{142} and the iron center. The ligand-free structures of wtHAO reported were refined at higher resolutions; therefore the water cluster in the mutant structure is less likely because of resolution differences. It appears that mutation of I142 disrupts a water-free, putative oxygen binding channel connecting protein surface to the catalytic iron ion. Therefore, the K_m values for O_2 of I142A and I142P increased dramatically.

Discussion

Protein dynamics during HAO reaction

Molecular oxygen is known to have a central role in complex living systems. Understanding how nature is able to selectively utilize O_2, a nonpolar reagent, to perform specific chemistry in aqueous solution at a high rate of catalysis is a question of great fundamental importance and deserving of study (1). It is apparent that the substrate of HAO, 3-HAA, with three polar functional groups, has considerable hydrophilic character. After binding with hydrophilic 3-HAA, how the HAO binary complex attracts a second, hydrophobic substrate is a question of fundamental importance. Here, we demonstrated that binding of 3-HAA induces loop dynamics of HAO to move to make for a more hydrophobic environment to efficiently capture molecular oxygen. The protein dynamic conformational change has loop regions moving by 8.6 Å and totally involves more than 15% of the protein residues in HAO. It is historically believed that O_2 would randomly diffuse into the protein scaffold, and enzymes that utilize O_2 have evolved to develop interior hydrophobic regions for O_2 binding. HAO presents a more intelligent way to facilitate O_2 binding to its active site. The O_2-binding channel is not permanently composed; it is dynamically formed in response to substrate binding and changes along with the reaction process. Presumably, the open conformation is for exchange of substrate and product, and the closed conformation is for rapidly incorporating oxygen.

The putative O_2 binding cavity in the active site of HAO

The loop regions covering the active site of HAO form an apparently dynamic hydrophobic cavity. In the ternary complex of HAO-ClHAA-O_2 structure, this is where the O_2 binds with one of the oxygen atoms anchored at the catalytic iron ion. The cavity in the ligand-free, open-form HAO structure (Fig. S9*A*) appears to be connected with the solvent from two different directions, potentially serving as a tunnel to facilitate ligand binding to the active site. In contrast, the cavity in the closed form wtHAO structure (Fig. S9*B*) exhibited significant differences as compared with the open form. The radius of the cavity decreases by approximately half, and the cavity no longer connects to the bulk solvent, presumably to minimize the impact of bulk solvent to the reactive intermediates during the catalytic reaction.

As was mentioned previously, Ile^{142} and Asn^{27} are located ~9 and 11 Å away from the catalytic iron ion, respectively. Elimination of the hydrogen-bonding interaction between loops A and C (mutant N27A) creates a variant that does not show the closed conformation upon substrate binding. The catalytic efficiency (k_{cat}/K_m) of N27A for both molecular oxygen and 3-HAA is dramatically decreased compared with WT (Table 1). The hydrogen bond formed between Asn^{27} and Ile^{142} is hypothesized to be the driving force to gather the loop regions together, which is triggered by the chelation of 3-HAA or ClHAA. Therefore, the dynamic action of the loop regions are critical for efficiently performing the dioxygenation. Meanwhile, the decreased hydrophobic character of loop region C (mutant I142A) could also lead to the elimination of loop movement, and determination of kinetic parameters with respect to oxygen is not possible. Without the proper positioning of Asn^{27} and Ile^{142}, the movement of loop regions A, B, and C would not occur, so the hydrophobic environment made by the "closed" form of the loop regions is broken, which leads to the reduction of oxygen capturing capacity of the mutants. Therefore, the major contribution of the loop regions is providing a sealed hydrophobic environment for binding and activation.

The loop regions in HAO from other biological origins

A comparison of available structures of 3-HAA dioxygenases can be found in Fig. S10. With the exception of an extra domain in HAO from mammalian sources, the overall structures show high similarity from a broad range of species. Compared with HAO from *C. metallidurans*, the RMSD values of HAO from *Homo sapiens*, *Bos taurus*, and *Saccharomyces cerevisiae* are 0.594, 0.813, and 1.072 Å, respectively. Moreover, the loop regions are among the highly conserved regions. Therefore, the loop regions required for the dioxygenation of HAO are one of the conserved structural characteristics during the evolution of HAO. Interestingly, holo-HAO from bovine crystallized in the closed form with a hydrogen bond between Asn^{24} and Leu^{137} (5). The isoleucine from loop C in prokaryotes is replaced by another similar residue of leucine in HAO from several eukaryotes (Fig. 1*D*). Based the alignment results, it is reasonable to believe that the dynamic action of loop regions for attracting hydrophilic or hydrophobic substrates has been conserved in HAOs during evolution.

How do the nonheme iron enzymes handle two or more substrates with distinct polar natures?

It is common in dioxygenases that flexible loop region movement is induced by interactions with substrates to be more ordered to cover the active site. Such an enzyme–substrate interaction can be observed and visualized by X-ray crystallographic structure determination. In an extradiol dioxygenase LapB, a loop containing His^{248} and Tyr^{257} was reported to hydrogen bond with its substrate, causing lower flexibility in the ligand-bound form (14). These two residues have essential roles during catalysis. In quercetin 2,3-dioxygenase, after binding its substrate (flavonol), a flexible loop around the active site became more ordered to stabilize the loaded substrate, and then the activation of C2 atom of flavonol was made to bind oxygen (15).

The nonheme iron and α-ketoglutarate (αKG)-dependent enzyme family catalyzes a variety of chemical reactions coupled to the decarboxylation of αKG to succinate. They meet the similar challenge of dealing with both a hydrophilic substrate (αKG or other substrates) and a hydrophobic substrate (oxygen). The common strategy is that they usually react with oxygen after binding a primary substrate. Taurine and αKG-dependent dioxygenase catalyzes taurine to aminoacetaldehyde and sulfite. Structural comparison reveals that the binding of taurine induced an α-helix region containing hydrophobic residues to move forward to the active site by forming a hydrogen-bonding network (16). The strategy of conformational change around the active site is similar with that of HAO. The α-helix region would help to form a more hydrophobic environment in the active site and benefit the capture of oxygen for performing the dioxygenation. The CurA halogenase also belongs to the nonheme Fe(II)/αKG–dependent family (17) and catalyzes a cryptic chlorination on a specific acyl carrier protein. Their crystal structures with various states indicate "open" and "closed" conformations. After binding with αKG, the disordered "lid" (open form) containing 27 residues on the top of the active site became a more ordered closed form, which was triggered by the salt bridge between αKG and Arg^{241}. The open form was proposed to organize the binding sequence in which the cosubstrate αKG and Cl^- need to bind to the iron ion prior to the oxygen and the acyl carrier protein. Although the lid region does not contain a high percentage of hydrophobic residues, its dynamic action is critical for the chlorination.

Phenylalanine hydroxylase (PAH) is a nonheme iron- and pterin-dependent enzyme that catalyzed the oxidation of phenylalanine to tyrosine. PAH binds pterin and L-Phe first and oxygen (hydrophobic) last (18). Structural study reveals that binding of pterin in the active site of PAH induces a loop region to move in the direction of the iron center by forming hydrogen-bond networks with the residues on the loop. Therefore, the PAH–pterin complex provides an ideal orientation for binding oxygen in between pterin and the iron ion (19).

Unlike the nonheme iron-dependent enzymes mentioned above, the loop regions in HAO do not have an obvious interaction with 3-HAA in the active site; rather they provide a hydrophobic environment for the dioxygenation caused by the high percentage of nonpolar residues in the loop regions. For other dioxygenases, including catechol dioxygenase, 2,3-dihydroxybiphenyl dioxygenase, biphenyl dioxygenase, and cysteine dioxygenase, substrate binding-induced loop region movement has not been reported or does not exist.

Structural requirement for capturing O_2 in iron-dependent proteins

The most well characterized oxygen binding to an iron protein is in heme systems. Hemoglobin is well known as an oxygen-transport metalloprotein in the blood cells, carrying oxygen from the respiratory organs to the rest of the body. Because of the functional requirement, hemoglobin has a high oxygen-binding capacity (20). The relationship between the oxygen-binding and structural information has been investigated since the hemoglobin crystal structures were determined. The histidine gate hypothesis was proposed by Perutz and Mathews (21) to demonstrate the HisE7 in the distal region controls the ligand migration rate by a conformation change from an open to a closed status. Boechi *et al.* (22) described that the hydrophobic effect around HisE7 is the major driving force for oxygen uptake other than steric hindrance from HisE7. Moreover, Cohen and Schulten (23) compared the characters of O_2 migration pathway in 12 monomeric globins from a broad range of species. The pathway for O_2 migration shows various configurations from different globins; however, the located residues are conserved as mainly containing hydrophobic residues (Trp, Phe, Leu, Ile, etc.). Therefore, the hydrophobic environment of cavity networks of globins facilitate ligands traveling through the protein matrix.

Concluding remarks

Although nature has more than one strategy to solve the low-oxygen-concentration problem in solution for a rapid oxygen consumption reaction at the enzyme active site, the unique feature of protein dynamics induced by substrate binding reported here may be the first structurally defined example for facilitating O_2 binding to the catalytic iron along with the primary organic substrate in each catalytic cycle. With a rapid turnover rate, the O_2 level could drop significantly after several seconds of oxygenation reaction, and the O_2 diffusion to the solution may not be fast enough and thus may cause a seemingly hypoxic condition. If this occurs, the increased hydrophobicity would become more important to attract O_2. Given the vast number of metal-dependent oxygen utilization enzymes, the protein dynamic-hydrophobicity strategy may be one of nature's common strategies to direct molecular oxygen toward organic substrate-bound metal centers.

Experimental procedures

Materials

The substrate 3-HAA and the inhibitor ClHAA were purchased from Sigma–Aldrich and Enamine Ltd. (Monmouth Jct., NJ), respectively.

Site-directed mutagenesis and protein preparation

The HAO gene from *C. metallidurans* was used as the template (GenBank™ accession no. CP000353) (3) to construct

single mutants by the PCR overlap extension mutagenesis method. The forward primers were 5′-TTGAAGCCGCCCGTCGGCGCCCGGCAGGTGTGGCAGGAC for N27A and 5′-GAGGTGCAGCTCAAGAGCGCCGTCACCGACCTCCCGCCT for I142A, and 5′-GAGGTGCAGCTCAAGAGCCCGGTCACCGACCTCCCGCC for I142P. The plasmids of mutants were verified and transformed to the expression host cells, *Escherichia coli* BL21(DE3). The purification strategy of the two mutants' proteins was the same as wtHAO (3). The wtHAO and mutants were anaerobically reconstituted with 3 eq. $Fe(NH_4)_2(SO_4)_2$ and excess Fe^{2+} was removed by Superdex 75 column before performing kinetic assay and crystallization.

Kinetic assay of wtHAO and mutants toward both substrates

The kinetic assays for wtHAO and mutants toward the substrate of 3-HAA were measured by monitoring the absorbance increase caused by the product formation (α-amino-β-carboxymuconate-ε-semialdehyde, $\epsilon_{360\,nm} = 47{,}500\ M^{-1}\ cm^{-1}$) with an Agilent 8453 diode-array spectrophotometer (3, 13). The O_2-saturated buffer was made through bubbling with pure oxygen gas during the analysis. The kinetic assays toward the substrate of oxygen were monitored with a Clark-type oxygen electrode (Oxygraph, Hansatech Instruments) with saturating 3-HAA concentration. All assays were done at room temperature.

Crystallization, data collection, processing, and refinement

The mutants were crystallized by the hanging-drop method in an anaerobic chamber as described previously (3, 13). After incubation with 20 mM of the inhibitor ClHAA for ~5–20 min, the soaked crystals were flash-cooled in liquid nitrogen. The diffraction data sets were collected, processed, and scaled by HKL-2000 (24). The structures of mutants were solved by molecular replacement by using the wtHAO (PDB entry 4L2N) as the template and refined by employing the Phenix 1.11.1–2575 (25) and Coot 0.8.3 (26). PyMOL (27) was used in drawing structural figures.

Author contributions—Y. Y. resources; Y. Y. and F. L. data curation; Y. Y. software; Y. Y. and F. L. formal analysis; Y. Y., F. L., and A. L. investigation; Y. Y., F. L., and A. L. visualization; Y. Y., F. L., and A. L. methodology; Y. Y., F. L., and A. L. writing-original draft; F. L. and A. L. conceptualization; F. L. and A. L. supervision; F. L. and A. L. validation; F. L. and A. L. project administration; F. L. and A. L. writing-review and editing; A. L. funding acquisition.

Acknowledgments—We thank Drs. Tadhg P. Begley and Steven E. Ealick for providing the HAO expression plasmid. We are indebted to Ian Davis for constructive discussions and manuscript editing. We thank the staff scientists at the sections 19 and 22 beamlines of the Advanced Photon Source (APS), Argonne National Laboratory and the beamline 9–2 of the Stanford Synchrotron Radiation Lightsource (SSRL), SLAC National Accelerator Laboratory. Use of the APS and SSRL is supported by the U.S. Department of Energy, Office of Science, Office of Basic Energy Sciences, under Contracts DE-AC02-06CH11357 and DE-AC02-76SF00515, respectively. The SSRL facility is additionally supported by National Institutes of Health Grant P41GM103393.

References

1. Kovaleva, E. G., and Lipscomb, J. D. (2008) Versatility of biological non-heme Fe(II) centers in oxygen activation reactions. *Nat. Chem. Biol.* **4,** 186–193 CrossRef Medline
2. Kovaleva, E. G., Neibergall, M. B., Chakrabarty, S., and Lipscomb, J. D. (2007) Finding intermediates in the O_2 activation pathways of non-heme iron oxygenases. *Acc. Chem. Res.* **40,** 475–483 CrossRef Medline
3. Zhang, Y., Colabroy, K. L., Begley, T. P., and Ealick, S. E. (2005) Structural studies on 3-hydroxyanthranilate-3,4-dioxygenase: the catalytic mechanism of a complex oxidation involved in NAD biosynthesis. *Biochemistry* **44,** 7632–7643 CrossRef Medline
4. Li, X., Guo, M., Fan, J., Tang, W., Wang, D., Ge, H., Rong, H., Teng, M., Niu, L., Liu, Q., and Hao, Q. (2006) Crystal structure of 3-hydroxyanthranilic acid 3,4-dioxygenase from *Saccharomyces cerevisiae*: a special subgroup of the type III extradiol dioxygenases. *Protein Sci.* **15,** 761–773 CrossRef Medline
5. Đilović, I, Gliubich F., Malpeli, G., Zanotti, G., and Matković-Čalogović, D. (2009) Crystal structure of bovine 3-hydroxyanthranilate 3,4-dioxygenase. *Biopolymers* **91,** 1189–1195 CrossRef Medline
6. Schwarcz, R. (2004) The kynurenine pathway of tryptophan degradation as a drug target. *Curr. Opin. Pharmacol.* **4,** 12–17 CrossRef Medline
7. Schwarcz, R., Bruno, J. P., Muchowski, P. J., and Wu, H.-Q. (2012) Kynurenines in the mammalian brain: when physiology meets pathology. *Nat. Rev. Neurosci.* **13,** 465–477 CrossRef Medline
8. Stone, T. W., and Darlington, L. G. (2002) Endogenous kynurenines as targets for drug discovery and development. *Nat. Rev. Drug Discov.* **1,** 609–620 CrossRef Medline
9. Kurnasov, O., Goral, V., Colabroy, K., Gerdes, S., Anantha, S., Osterman, A., and Begley, T. P. (2003) NAD biosynthesis: identification of the tryptophan to quinolinate pathway in bacteria. *Chem. Biol.* **10,** 1195–1204 CrossRef Medline
10. Colabroy, K. L., and Begley, T. P. (2005) Tryptophan catabolism: identification and characterization of a new degradative pathway. *J. Bacteriol.* **187,** 7866–7869 CrossRef Medline
11. Muraki, T., Taki, M., Hasegawa, Y., Iwaki, H., and Lau, P. C. (2003) Prokaryotic homologs of the eukaryotic 3-hydroxyanthranilate 3,4-dioxygenase and 2-amino-3-carboxymuconate-6-semialdehyde decarboxylase in the 2-nitrobenzoate degradation pathway of *Pseudomonas fluorescens* strain KU-7. *Appl. Environ. Microbiol.* **69,** 1564–1572 CrossRef Medline
12. Colabroy, K. L., Zhai, H., Li, T., Ge, Y., Zhang, Y., Liu, A., Ealick, S. E., McLafferty, F. W., and Begley, T. P. (2005) The mechanism of inactivation of 3-hydroxyanthranilate-3,4-dioxygenase by 4-chloro-3-hydroxyanthranilate. *Biochemistry* **44,** 7623–7631 CrossRef Medline
13. Liu, F., Geng, J., Gumpper, R. H., Barman, A., Davis, I., Ozarowski, A., Hamelberg, D., and Liu, A. (2015) An iron reservoir to the catalytic metal: the rubredoxin iron in an extradiol dioxygenase. *J. Biol. Chem.* **290,** 15621–15634 CrossRef Medline
14. Cho, J.-H., Jung, D.-K., Lee, K., and Rhee, S. (2009) Crystal structure and functional analysis of the extradiol dioxygenase LapB from a long-chain alkylphenol degradation pathway in *Pseudomonas*. *J. Biol. Chem.* **284,** 34321–34330 CrossRef Medline
15. Steiner, R. A., Kalk, K. H., and Dijkstra, B. W. (2002) Anaerobic enzyme substrate structures provide insight into the reaction mechanism of the copper-dependent quercetin 2,3-dioxygenase. *Proc. Natl. Acad. Sci. U.S.A.* **99,** 16625–16630 CrossRef Medline
16. O'Brien, J. R., Schuller, D. J., Yang, V. S., Dillard, B. D., and Lanzilotta, W. N. (2003) Substrate-induced conformational changes in *Escherichia coli* taurine/α-ketoglutarate dioxygenase and insight into the oligomeric structure. *Biochemistry* **42,** 5547–5554 CrossRef Medline
17. Khare, D., Wang, B., Gu, L., Razelun, J., Sherman, D. H., Gerwick, W. H., Håkansson, K., and Smith, J. L. (2010) Conformational switch triggered by α-ketoglutarate in a halogenase of curacin A biosynthesis. *Proc. Natl. Acad. Sci. U.S.A.* **107,** 14099–14104 CrossRef Medline
18. Volner, A., Zoidakis, J., and Abu-Omar, M. M. (2003) Order of substrate binding in bacterial phenylalanine hydroxylase and its mechanistic implication for pterin-dependent oxygenases. *J. Biol. Inorg. Chem.* **8,** 121–128 CrossRef Medline

19. Erlandsen, H., Bjørgo, E., Flatmark, T., and Stevens, R. C. (2000) Crystal structure and site-specific mutagenesis of pterin-bound human phenylalanine hydroxylase. *Biochemistry* **39,** 2208–2217 CrossRef Medline
20. Dominguez de Villota, E. D., Ruiz Carmona, M. T., Rubio, J. J., and de Andrés, S. (1981) Equality of the *in vivo* and *in vitro* oxygen-binding capacity of haemoglobin in patients with severe respiratory disease. *Br. J. Anaesth.* **53,** 1325–1328 CrossRef Medline
21. Perutz, M. F., and Mathews, F. (1966) An X-ray study of azide methaemoglobin. *J. Mol. Biol.* **21,** 199–202 CrossRef Medline
22. Boechi, L., Arrar, M., Martí, M. A., Olson, J. S., Roitberg, A. E., and Estrin, D. A. (2013) Hydrophobic effect drives oxygen uptake in myoglobin via histidine E7. *J. Biol. Chem.* **288,** 6754–6762 CrossRef Medline
23. Cohen, J., and Schulten, K. (2007) O_2 migration pathways are not conserved across proteins of a similar fold. *Biophys. J.* **93,** 3591–3600 CrossRef Medline
24. Otwinowski, Z., and Minor, W. (1997) Processing of X-ray diffraction data collected in oscillation mode. *Methods Enzymol.* **276,** 307–326 CrossRef
25. Adams, P. D., Afonine, P. V., Bunkóczi, G., Chen, V. B., Davis, I. W., Echols, N., Headd, J. J., Hung, L.-W., Kapral, G. J., Grosse-Kunstleve, R. W., McCoy, A. J., Moriarty, N. W., Oeffner, R., Read, R. J., Richardson, D. C., *et al.* (2010) PHENIX: a comprehensive Python-based system for macromolecular structure solution. *Acta Crystallogr. D Biol. Crystallogr.* **66,** 213–221 CrossRef Medline
26. Emsley, P., and Cowtan, K. (2004) Coot: model-building tools for molecular graphics. *Acta Crystallogr. D Biol. Crystallogr.* **60,** 2126–2132 CrossRef Medline
27. DeLano, W. L. (2014) *The PyMOL Molecular Graphics System*, version 1.7.0.0, Schrodinger, LLC, New York
28. Karplus, P. A., and Diederichs, K. (2012) Linking crystallographic model and data quality. *Science* **336,** 1030–1033 CrossRef Medline
29. Engh, R. A., and Huber, R. (1991) Accurate bond and angle parameters for X-ray protein structure refinement. *Acta Crystallogr. A* **47,** 392–400 CrossRef
30. Chen, V. B., Arendall, W. B., 3rd, Headd, J. J., Keedy, D. A., Immormino, R. M., Kapral, G. J., Murray, L. W., Richardson, J. S., and Richardson, D. C. (2010) MolProbity: all-atom structure validation for macromolecular crystallography. *Acta Crystallogr. D Biol. Crystallogr.* **66,** 12–21 CrossRef Medline
31. Robert, X., and Gouet, P. (2014) Deciphering key features in protein structures with the new ENDscript server. *Nucleic Acids Res.* **42,** W320–W324 CrossRef Medline

Adapting to oxygen: 3-Hydroxyanthrinilate 3,4-dioxygenase employs loop dynamics to accommodate two substrates with disparate polarities

Yu Yang, Fange Liu and Aimin Liu

J. Biol. Chem. 2018, 293:10415-10424.
doi: 10.1074/jbc.RA118.002698 originally published online May 21, 2018